# Multiscale Modeling of Sub-Entanglement-Scale Chain Stretching and Strain Hardening in Deformed Polymeric Glasses

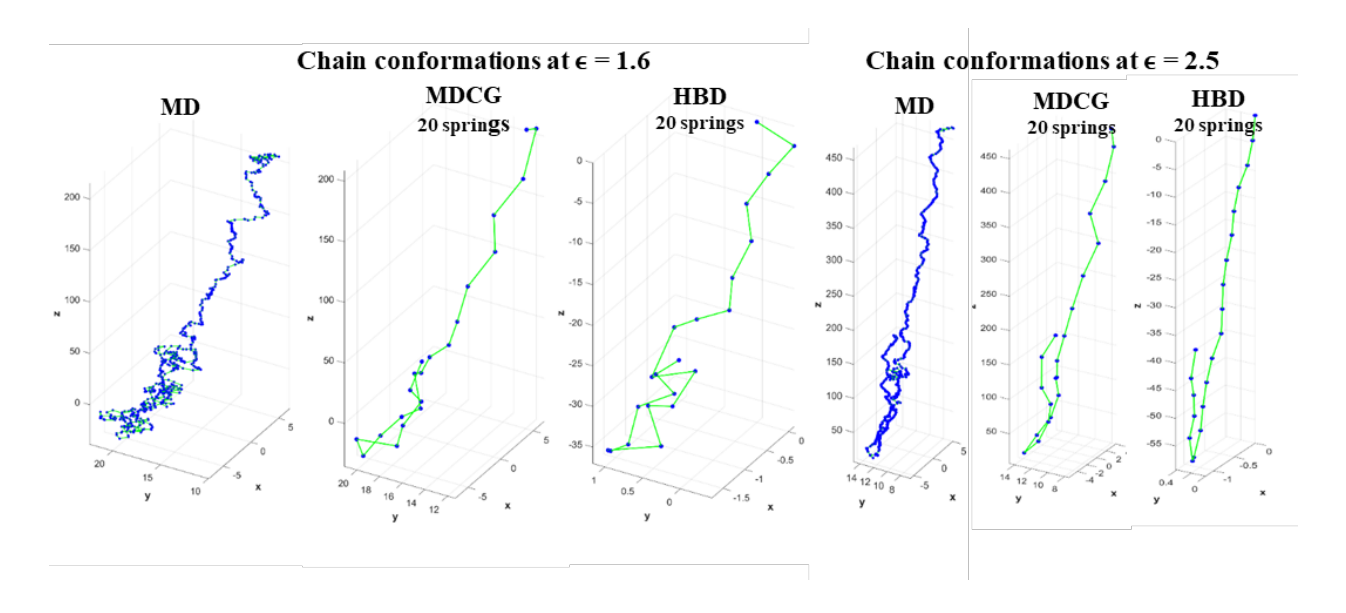
Weizhong Zou#, Soroush Moghadam+, Robert S. Hoy<sup>‡\*</sup>, Ronald G. Larson<sup>#\*\*</sup>

- # Department of Chemical Engineering, University of Michigan, Ann Arbor, MI 48109
- + Department of Mechanical Engineering, University of Michigan, Ann Arbor, MI 48109 ‡ Department of Physics, University of South Florida, Tampa, FL 33620

\*Correspondence: email: <u>rlarson@umich.edu</u>, phone: (734) 936-0772, FAX: (734) 763-0459

\*\*Correspondence: email: <u>rshoy@usf.edu</u>, phone: (813) 974-0063, FAX: (813) 974-5318

# For Table of Contents Use Only



### **Abstract**

Using both coarse-grained (CG) and fine-grained (FG) simulations we show how strain hardening in polymeric glasses under uniaxial extension arises from highly stretched strands that form as the polymer chains deform subaffinely on increasing length scales as strain increases. The coarsegrained simulations are performed using the hybrid Brownian Dynamics method (HBD) [Zou, W. & Larson, R. G. Soft Matter 2016, 3, 3853-3865] with 10-30 coarse-grained springs per polymer chain, while the fine-grained simulations employ the Kremer-Grest bead-spring model with 600 beads per chain. We find that the HBD model accurately predicts how the MD chain configurations evolve during deformation despite being a single-chain-in-mean-field model that does not account for entanglements or monomer-level structure. We show using both models that the glassy strain hardening modulus  $G_R$  is much larger than the melt plateau modulus  $G_N$  because chain segments become highly stretched at modest Hencky strain ( $\epsilon < \sim 1$ ) owing to the high interchain friction in the glass. HBD model predictions of strain hardening match those of the MD simulations in shape and magnitude, relative to the flow stress, which is the stress just beyond the yield point, for several deformation protocols, and also capture the increase in strain hardening with increasing chain length that saturates in the long chain limit. As deformation proceeds, chains begin to form kinks or folds (starting at a Hencky strain  $\epsilon \sim 1.6$ ) analogous to those produced in extensional flows of dilute and entangled polymer solutions. We identify "entangled kinks" in the MD simulations; these do not appear to strongly influence strain hardening, but may be important in delaying fracture. Motivated by these results, we improve upon HBD's ability to accurately capture stressstrain curves at small strains through yielding and strain softening by extending the theory to multiple segmental relaxation modes, whose strain-dependent relaxation times are obtained from small-molecule probe relaxation experiments by Ediger and coworkers [Bending, B. & Ediger, M. D. J. Polym. Sci. B 2016, 54, 1957-1967]. This produces excellent agreement between the HBD

model and experimental stress-strain curves through the yield point, but requires segmental relaxation data for each experiment. Future work should aim at developing a constitutive equation for the segmental relaxation.

### Introduction

Glassy materials possess remarkable properties such as high stiffness and transparency, good corrosion resistance, low permeability, as well as ease of fabrication, 1-2 making them ubiquitous in both traditional and emerging material applications.<sup>3,4,5,6</sup> The growing demand for low-cost, lightweight materials with sufficient mechanical strength has led to increasing use of polymeric glasses as substitutes for inorganic materials such as silicon and metals. However, polymeric glasses tend to fail in a catastrophic, brittle fashion through avalanche-like plastic deformation, often manifested as crazing and necking. This often makes their ductility significantly lower than that of conventional metals, which can render them useless for many applications. <sup>7</sup> To ensure their mechanical stability for a variety of loading environments, several methods for strengthening polymeric glasses are available, for example, mechanical preconditioning, 8,9 subglass-transitiontemperature annealing, 10 etc. However, the complicated interplay of chemistry, 11,12 entanglement/crosslink density, <sup>13</sup> severity of confinement, <sup>14</sup> as well as thermomechanical history in determining ultimate mechanical properties of polymeric glasses make it extremely difficult to ensure the above stability-enhancing procedures are reliable.<sup>4,5,15</sup> Moreover, the still-rapid pace of development of new glasses with remarkable performance, including vapor-deposited "ultrastable" polymer glasses, plasticizer-mediated glasses, and rigid polymer-cast "superionic" films, 16 show that we are still far from a complete understanding of how polymers' molecular structure affects the macroscopic mechanical properties of their bulk glassy state. For example, while it is well known that the restrictions imposed by the strength and directionality of covalent bonds along chain backbones (which distinguish polymeric from small-molecule glasses) play a critical role when a polymer glass is subjected to large strains,<sup>3,17-19</sup> the details remain highly

controversial.<sup>20,21</sup> Progress towards predicting the performance of polymeric glasses under large deformation therefore requires an explicit accounting both short-range segmental dynamics and long-range polymeric ones, as well as the interaction of the two.

Glasses composed of short polymer chains are prone to brittle fracture, while those composed of well-entangled chains are usually more ductile, especially if they exhibit pronounced post-yield strain hardening.<sup>22</sup> Understanding the source of strain hardening is thus a reasonable starting point for improving the strength of polymeric materials. Molecular dynamics simulations are particularly useful in this effort because they provide complete detail on chain configurations, local strain variations, multiscale anisotropy, and any other measure of plastic deformation one can imagine. Targeted coarse-grained simulations<sup>7,23-30</sup> have also been used to investigate glassypolymeric strain hardening in considerable detail over the past decade. Three results from these simulations that are potentially critical for achieving a general understanding of strain hardening are: (i) For strains between yield and the onset of supralinear, "Langevin" hardening, the stress  $\sigma$ is primarily dissipative (viscoplastic); (ii) for any given polymer, although the plastic flow stress  $\sigma_f$  and strain hardening modulus  $G_R$  each depend significantly on temperature and strain rate, they remain linearly related to each other as these parameters are varied; (iii) in bidisperse mixtures where a weight fraction f of chains have length  $N < N_e$  and the remaining chains have length N >> $N_e$  (where  $N_e$  is the rheological entanglement length measured in number of monomers),  $\sigma(\epsilon) \sim 0$  $f\sigma_{short}(\epsilon) + (1-f)\sigma_{long}(\epsilon)$ , where  $\sigma_{short}(\epsilon)$  and  $\sigma_{long}(\epsilon)$  are the respective responses for f = 1 and f = 0, up to the onset of Langevin hardening. Results (i-ii) are corroborated by experiments. 31,32 While result (iii) is difficult to test directly for  $f > \sim 0.5$  owing to the tendency of short chains to produce

defects that lead to brittle fracture in experiments,<sup>33</sup> it is consistent with Kramer's argument<sup>20</sup> that entropic elasticity is not the primary source of strain hardening.

The least-well-understood aspect of strain hardening is the physical origin of the ratio  $F(\epsilon) = \sigma(\epsilon)/\sigma_f$  for large strains. Haward suggested<sup>34</sup> that  $G_R >> G_N$  because the magnitude of  $G_R$  is set by the density of uncrossable chain contours  $\rho_c$ , which is much larger than the entanglement density  $\rho_e$ . Both these densities increase with chain stiffness, as does  $F(\epsilon)$ .<sup>34</sup> In neat high-polymer glasses,  $G_R$  depends linearly on entanglement density,<sup>35</sup> which suggests that entanglements dominate hardening in glasses just as they do in rubbers. This assumption has been employed in many models of glassy polymer mechanics, including the highly successful 8-chain model of Arruda and Boyce.<sup>36</sup> On the other hand, in bidisperse mixtures  $\rho_e$  and  $G_N$  are quadratic in (1-f), but [ $F(\epsilon)$  -1] is linear in (1-f),<sup>24</sup> which suggests that entanglements are less important. In fact, the linear dependence of hardening modulus on long-chain weight fraction suggests that hardening results from stresses produced by individual chains deforming in a very viscous medium.<sup>24</sup>

Taken together, results (i-iii) imply that much of glassy-polymeric strain hardening response can be captured by theories in which a glass-physics model for the segment-scale dynamics is coupled to a single-chain-in-mean-field model for the large-scale chain configurations. Such models reflect the fact that the primary forces in polymer glasses are short-ranged and the evolution of chain-scale structure under deformation is strongly coupled to the evolution of segment-scale structure. In fact, there are a number of recently developed coarse-grained theoretical models<sup>37-42</sup> for polymer glasses that are constructed along these lines. Two of us (Zou and Larson) recently published one such coarse-grained "hybrid" model<sup>43-45</sup> in which a one-mode Maxwellian equation for local

segmental relaxation with time constant  $(\tau^s)$  was used to predict the local frictional drag that a "glassy solvent" exerts on an isolated-chain representing the larger-scale "polymeric" relaxation (with time constant  $\tau^p = \alpha \tau^s$ , where  $\alpha$  is the polymer-to-segmental relaxation time ratio). With a simple fluidity model describing the nonlinear response of  $\tau^s$  under applied deformation, the stress from the segmental mode was added to that produced by polymeric relaxation, whose dynamics were approximated by a bead-spring chain with bead drag coefficient proportional to  $\tau^s$ . Although the interplay between segmental and polymeric stresses allows this hybrid model to capture much of the experimental phenomenology of deformed polymeric glasses, 43-45 the model ignores entanglements. It also ignores specific energetic terms arising from pair, covalent-bond, and angular interactions, all of which are known to be important in determining the overall mechanical properties of polymeric glasses. One might therefore expect this model to break down in the postyield regime, where effects of these energetic terms become increasingly important. <sup>26,28,31</sup> On the other hand, there is considerable evidence that single-chain-in-mean-field models can in fact capture much of the physics of large-strain deformation, including strain hardening, at least up to the beginning of the "dramatic" (supra-Gaussian) hardening regime. Moreover, our recent work<sup>45</sup> suggests that Gaussian strain hardening in glasses results primarily from highly-stretched subchains separated by bends or nascent fold points rather than from entanglements. Significantly, the model<sup>45</sup> correctly predicts the onset of strain hardening at Hencky strains of order unity and that the hardening modulus  $G_R$  is much greater than the melt plateau modulus  $G_N$ . These findings suggest that the most important cause of strain hardening is the large stretch of sub-entangled strands of polymer chains that arises because the applied deformation rate is much greater than the rate at which those strands can relax their configurations. Unfortunately it is not yet possible to test this idea experimentally, despite the applications of many novel experimental methods to

deformed polymeric glasses.<sup>5,10,47,49</sup> MD simulations, however, offer an alternative avenue for exploring and testing new theories, and can provide information on polymer conformations and entanglements.<sup>7,48</sup> In particular, they allow testing of the assumptions and findings of our coarsegrained hybrid-BD (HBD) model, and specifically its ability to predict coarse-grained chain configurations and strain hardening accurately despite neglecting entanglements and local polymer chain structure. Thus, in the following sections, we will find the extent to which chain deformation and stress predicted by a Kremer-Grest bead-spring MD simulation can be captured by a much coarser grained hybrid Brownian dynamics model (HBD) that is resolved at the level of 10 or more Kuhn steps.

#### **Simulation Methods**

Molecular Dynamics (MD) Simulations. Our standard MD simulations use a flexible Kremer-Grest bead-spring glass,  $^{51,52}$  consisting of  $N_{ch} = 500$  chains of length  $N_{MD} = 600$  monomer beads. Since the Kuhn length of this model is  $\sim 5/3$  beads, each chain has  $N_K = 360$  Kuhn segments with entanglement length  $N_e \sim 51$  Kuhn segments,  $^{13}$  so that a chain has an average of 7-8 entanglements. All monomers have mass m and interact via the truncated and shifted LJ potential  $U_{LJ}(r) = 4u_0$ .  $[(a/r)^{12} - (a/r)^6 - (a/r_c)^{12} + (a/r_c)^6]$ , where  $u_0$  is the intermonomer binding energy, a is the monomer diameter and  $r_c = 2^{7/6}a$  is the cutoff radius. Covalent bonds are modeled using the FENE potential  $U_{FENE}(r) = -(kR_0^2/2) \cdot \ln[1 - (r/R_0)^2]$  with the standard parameter  $^{51}$  choices  $R_0 = 1.5a$  and  $k = 30u_0/a^2$ . The Lennard-Jones time unit is  $\tau = (ma^2/u_0)^{1/2}$ , and the MD time step we employ is  $\Delta t = 0.005\tau$ . As in Ref. 29, the system is first thoroughly equilibrated well above  $T_g$  (at  $T = 0.47u_0/k_B \sim 1.3T_g$ ),  $^{52}$  then slowly cooled to  $T = 0.3u_0/k_B \sim 0.8T_g$ . Since the cooling rate employed for  $T < T_g + 0.1u_0/k_B$ 

is  $10^{-6}u_0/k_B\tau$ , the aging time  $(t_w)$  of the glass, approximated as the time between attainment of the glass transition at  $T_g = 0.37u_0/k_B$  and the final temperature  $T = 0.3u_0/k_B$  is  $0.07\tau/10^{-6} = 7\times10^4\tau$ . After cooling the system, we uniaxially stretch the box containing the chains at a rate of  $\dot{\epsilon} = 2.5\times10^{-5}/\tau$  while symmetrically reducing its transverse dimensions to maintain constant volume. Thus, the strain rate times the aging time is  $\dot{\epsilon}t_w = 1.75$ , which is close to unity. Throughout all these simulations, periodic boundaries are applied along all three directions; the monomer number density of the  $T = 0.3u_0/k_B$  glass is  $\rho = 1.0578/a^3$ . All MD simulations are performed using LAMMPS.<sup>53</sup>

Hybrid Brownian Dynamics (HBD) Simulations. On the other hand, for HBD simulations, the polymeric glass is represented by phantom bead-spring chains with extensible FENE springs, suspended in an implicit "glassy" solvent, with each bead acting as a center of force. The relaxation time of the glassy solvent is represented by a phenomenological fluidity equation, Eq. (1):

$$\dot{\tau}^{\scriptscriptstyle S} = 1 - \lambda (\tau^{\scriptscriptstyle S} - \tau^{\scriptscriptstyle S}_0) \quad (1a)$$

$$\lambda = \mu \sqrt{2tr(\boldsymbol{D}:\boldsymbol{D})}, \boldsymbol{D} = [\nabla \boldsymbol{v} + (\nabla \boldsymbol{v})^T]/2$$
 (1b)

Here,  $\tau_0^s$  is the fully rejuvenated relaxation time, which is fixed at the value of 6 s, which is far smaller than  $\tau^s$  and so its exact value is not very important.  $\mathbf{D}$  is the deformation rate tensor, and  $\nabla \mathbf{v}$  is the velocity gradient. The rejuvenation parameter  $\mu$  influences the strain required for the glassy mode to "rejuvenate" and become liquid-like under deformation. This parameter controls plasticity and local properties of the glass; in particular, it is roughly inversely proportional to the flow stress  $\sigma_f$  (which is the plateau stress immediately following the yield point), is inversely

proportional to the yield strain, and influences the formation of localized "kinks" or folds in the chain at high strain rate in the HBD model, as shown below.

Note that Eq. (1) is a highly oversimplified one-parameter model of physical ageing and rejuvenation that lacks detailed consideration of the thermomechanical history of the sample. In particular, the rate of rejuvenation is assumed to depend solely on strain-rate history, which will cause softening even in the linear viscoelastic regime at high frequencies. As we shall see, it leads to a stress overshoot on startup of flow that increases strongly with strain rate, rather than approximately logarithmically as in real glasses, and to a flow stress that is less sensitive to strain rate at high strain rates than seen in MD simulations. Eq. (1) is thus only (barely) suitable as a crude model for some simple nonlinear strain histories (See "Drawbacks of single-mode segmental model" in SI for details.) We will later replace this model with experimental measurements of segmental mode relaxation to predict the yielding behavior for an experimental PMMA glass. Future work should focus on the development, or adoption from the literature, of a better segmental model.

The total stress is given by the sum of polymeric and "segmental" contributions,  $\Sigma^p$  and  $\Sigma^s$ , where superscripts "p" and "s" represent "polymeric" or "segmental" mode, respectively. The segmental component satisfies an upper convected Maxwell model, with relaxation time  $\tau^s$  and modulus  $G^s$ . The polymeric stress  $\Sigma^p$  is obtained from the BD simulations of a bead-spring chain and assigned a modulus  $G^p$ . This modulus  $G^p$  is a modulus per coarse-grain spring in the model, as explained in the SI, and therefore is inversely proportional to the number of springs used in the model. For the 20-spring model used in most of the work here, with each spring constituting 18 Kuhn steps,  $G^p$ 

should be about twice the plateau modulus of the melt simulated by the MD method. The bead drag coefficient used in the HBD simulations of the polymer is made proportional to the instantaneous value of the segmental relaxation time  $\tau^s$  whose evolution is described by Eq. (1a). Since the polymer chain is a Rouse chain, its longest relaxation time  $\tau^p$  will be proportional to the square of the number of Kuhn steps in the chain  $N_K^2$ , times the local relaxation time of a single Kuhn segment  $\tau^K$ , which will depend on the stiffness of the polymer. Defining  $\alpha^K = \tau^K/\tau^s$ , the ratio  $\alpha \equiv \tau^p/\tau^s = \alpha^K N_K^2$  should therefore be proportional to the square of the chain length. We expect that it should increase with chain stiffness (for fixed  $N_K$ ). For flexible chains with  $N_K = 360$  (as employed in our MD simulations), assuming that  $\alpha^K = 1$  yields  $\alpha = 1.3 \times 10^5$ , which is close to the value we use here ( $\alpha = 8 \times 10^4$ ; see Table 1). Simulations are carried out after assigning an initial value,  $t_W$ , to  $\tau^s$ , called the "waiting time" since it is roughly the value of  $\tau^s$  achieved after the sample has rested for a time  $t_W$  following a previous strong deformation. It can also be considered the sample's "age." A detailed description of the model can be found in our previous work, <sup>45</sup> and additional details relevant to the present study are given in the SI.

As a result of coarse-graining, some of the parameters of the MD simulation are represented by different variables in the HBD model. The number of monomers N (or number of Kuhn steps  $N_K$ ) in the MD simulation is captured by the number of springs  $N_{HBD}$  of the HBD model along with the FENE spring force law, which is sensitive to the number of Kuhn steps  $N_{K,s}$  per spring.  $N_K$  in the MD simulations should be equal to the product  $N_{K,s} \times N_{HBD}$  of the HBD model. The chain density  $\rho$  of the MD model is captured in the polymer modulus  $G^p$  of the HBD model as explained in the SI (Eq. S4). The glass age of the MD model should be similar to the "waiting time"  $t_w$  of the HBD model. The temperature T of the MD model should influence both the glassy modulus  $G^s$  and the

rejuvenation parameter  $\mu$  of the HBD model in some way that is yet to be explored. Finally, a combination of the chain stiffness of the MD model, set by a bending potential, and the chain length N of the MD model, should be reflected in the value of  $\alpha$  in the BD model. While the link between the chain length N of the MD model and  $N_K$  of the HBD model is clear (as shown explicitly below), the relationship between the bending potential of the MD model and  $\alpha$  and possibly other parameters of the HBD model has yet to be worked out in detail.

### **Results and discussion**

To compare MD results directly with our HBD results where a modest number of springs ( $N_{HBD} = 10, 20, \text{ or } 30$ ) is used, the MD chain conformations need to be coarse-grained. We do this by first dividing the MD chain into  $N_{HBD}$  sequential subsections, each containing  $N_{MD}/N_{HBD}$  MD springs (i.e.,  $N_{MD}/N_{HBD} + 1$  MD beads), and then map each of these onto a single coarse-grained "MDCG" vector connecting the endpoints of the subsection. For the "base" case in which we use  $N_{HBD} = 20$  springs in the HBD model, we therefore map 30 MD beads with 18 Kuhn steps of an MDCG strand into a single HBD spring, and assign parameters to the spring so that it represents 18 Kuhn segments. Thus  $N_{MDCG} = (N_{HBD})$  is the number of strands (springs) in the MDCG (HBD) model. From the starting state of an MD simulation, we take an initial ensemble of chain configurations to form the MDCG strands, and use these coordinates to form HBD bead-spring chains. We then run these in an HBD simulation under fast extension so that large-scale chain relaxation is negligible, and the overall chain conformation and stress of our coarse-grained (HBD) and fine-grained (MD) models are only weakly dependent on the deformation rate. The "age" of the glassy mode of the HBD model is the "waiting time"  $t_w$ , which is set to 26.4 h = 9.5×10<sup>4</sup> s (see Table I).

A high extension rate of  $\dot{\epsilon} = 10^{-5} \, \mathrm{s}^{-1}$  is applied for HBD simulations giving  $\dot{\epsilon}t_w = 0.95$ , which is around unity, close to the corresponding value  $\dot{\epsilon}t_w = 1.75$  for the MD simulations discussed above, for which  $\dot{\epsilon} = 2.5 \times 10^{-5} / \tau$  and  $t_w = 7 \times 10^4 \tau$ . Since the relaxation time of the polymer chain  $\tau^p$  is many orders of magnitude longer than the relaxation time of the glassy mode, which is close to  $t_w$ , the value  $\dot{\epsilon}t_w$  of around unity implies that the Weissenberg number for the entire polymer  $\dot{\epsilon}\tau^p$  is very much higher than unity and nearly the same in both MD and HBD simulations. An example chain conformation at two Hencky strains  $\epsilon = 1.6$  and 2.5 from both MD and HBD simulations under uniaxial extension are shown in Fig. 1, with the values of the HBD parameters given in Table I. For this comparison, as described above, the starting configuration of the HBD chain at equilibrium was taken as that of the MDCG chain extracted from the MD initial configuration. The agreement in configuration as a function of strain between the two is typical of the majority of the chains, with more quantitative comparisons discussed in what follows.

Table 1. Standard values of model parameters for HBD simulations in Figs. 1-4.

ė (s <sup>-1</sup> )	α	$N_{HBD}$	μ	N <sub>K</sub>	<i>t</i> <sub>w</sub> (h)	G <sup>p</sup> (MPa)	Gs (MPa)
10 <sup>-5</sup>	8.0×10 <sup>4</sup>	20	143	360	26.4	0.67	500

The values used here for all parameters are the same as in our previous work,<sup>45</sup> except for  $\alpha$  and  $G^p$ . The value of  $\alpha$  is approximately  $N_K^2$ , consistent with the number of Kuhn lengths in the HBD and MD chains. And  $G^p$  (=  $3\rho RT/M_S$ ) is set as a typical value of the "spring modulus"  $G^p$ , where  $M_S$  is the molecular weight of a single spring. To represent a 18-Kuhn-step segment of polymer such as PMMA (a Kuhn-step molecular weight is around 611 Daltons with  $C_\infty$  = 8.22 and backbone bond molecular weight ~50 Daltons for PMMA),  $M_S$  = 11K Daltons, giving  $G^p \approx 0.67$  MPa (according to the formula for the polymer stress used in Eq. 4a of our previous paper<sup>45</sup>).  $N_K$  also was adjusted from that in the previous work slightly from 400 to 360, to match the value for the MD simulations.

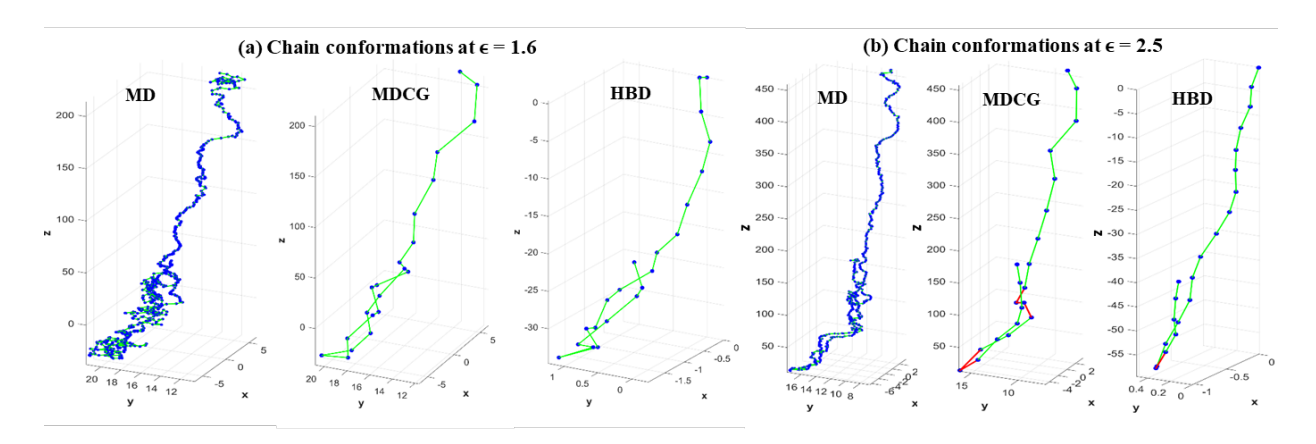


Figure 1. Chain conformations predicted from MD simulations with/without coarse-graining (i.e., MD and MDCG chains) under a constant extension rate of  $\dot{\epsilon} = 2.5 \times 10^{-5}$  in LJ units and from HBD simulations with  $N_{HBD} = 20$  under a constant extension rate of  $\dot{\epsilon} = 10^{-5}$  s<sup>-1</sup>, for an example chain at (a)  $\epsilon = 1.6$ ; (b)  $\epsilon = 2.5$ . Blue beads are connected via green springs for MD, MDCG and HBD chains. Each pair of adjacent red springs in (b) contains a local "fold" or "kink" discussed in the text. As discussed in the text, the product  $\dot{\epsilon}t_w \sim 1$  is nearly the same in both MD and HBD simulations. Qualitatively similar results are also obtained by changing the level of coarse-graining, e.g.  $N_{HBD} = 10$  or 30, as shown in the SI.

Non-affine Stretching, Mean Stretch, and Highly Stretched Segments. Figure 1 shows that the HBD simulations predict strain-dependent chain conformations similar to those produced in the MD simulations as long as the initial HBD configurations are obtained by coarse-graining the initial MD configuration. We quantify the ensemble-averaged strain-dependent configurations and their similarity between MD and HBD simulations in Fig. 2. Figure 2(a) shows that the mean-squared end-to-end distance of a strand containing n Kuhn segments follows affine deformation at large n, i.e.,  $\langle R_n^2 \rangle_{eq} = (e^{2\epsilon} + 2e^{-\epsilon})/3$  as a function of strain  $\epsilon$  in uniaxial extension, where  $\langle R_n^2 \rangle_{eq}$  is the mean-squared end-to-end distance at equilibrium. Although the deformation of a typical chain is essentially affine on large scales, the near-inextensibility of covalent bonds forces chains to deform sub-affinely on short scales. A continuous crossover from sub-affine to affine

deformation is shown by both HBD and MD results, with the crossover strand length n\* increasing with strain.<sup>28</sup> We find that even at small strain ( $\epsilon \sim 0.5$ ), subaffinity is significant for chain segments with n as large as  $\sim N_e/3$ , where  $N_e \sim 51$  is the number of MD Kuhn segments per entanglement. This result agrees with small angle neutron scatting (SANS) experiments<sup>54</sup> on glassy PMMA that had been deformed into the strain hardening regime, which showed a crossover from subaffine to affine deformation at a length scale of about  $\sim 1/2$  of the entanglement mesh size. Figure 2(b) shows MD and HBD results for the mean segmental stretch S(n) (=  $\langle R_n^2 \rangle^{0.5}/nb_K$ ). Here S(1) = 1 because covalent bonds are inextensible and  $S(n) \sim n^{-1/2}$  for large n because chains are random-walk-like. The key result illustrated here is that as the strain reaches unity and beyond, S(n) at the sub-entanglement scale increases dramatically. Figure 2(c) quantifies the fraction of "highly stretched chain segments"  $F_{hs}(n)$  that have  $S(n) > S_{min}$  (= 0.7). It is clear that  $F_{hs}$  becomes large around the onset of strain hardening (at  $\epsilon \sim 1.0$ , as shown later in Fig. 6), and well before fully-formed kinks/well-folded chains appear (at  $\epsilon \sim 1.6$ , see Figs. 3 and 4). We will show that it is these highly stretched chain segments (which appear as precursors to kinked or folded strands) that lead to the onset of strong strain hardening. While the HBD model in Fig. 2 uses  $N_{HBD} = 20$ coarse-grained springs corresponding to 30 MD beads/springs, the SI shows that the similarity between the MD and HBD chain configurations is insensitive to values of  $N_{HBD}$  between 10 and 30. As also shown in both the main text and the SI, the results in Fig. 2 are also insensitive to rejuvenation parameter  $\mu$  (Fig. 3) and to strain rate (Figs. S3-S6) for both the HBD and MD models. Although chain configurations are quite different in uniaxial compression than in extension (compare Figs. S7 and S8 to Figs. S1 and S2), there remains very good agreement between MD and HBD simulations in each case, with HBD parameters held fixed when strain rate or strain type

are changed. Results in the SI show good agreement between HBD and MD simulations for deformation affinity, strand stretch, and the fraction of highly stretched segments.

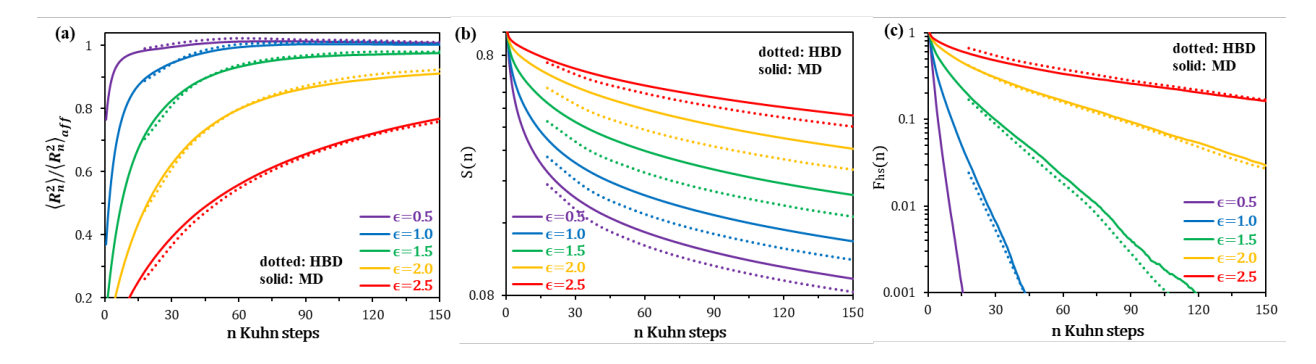


Figure 2. Local stretching in fine-grained Kremer-Grest polymer model (solid lines) compared to that of the coarse-grained HBD model (dotted lines) with  $N_{HBD} = 20$ . (a) The ratio of the mean-squared distance  $\langle R_n^2 \rangle$  between monomers separated by n Kuhn steps to its affine value  $\langle R_n^2 \rangle_{aff}$  as a function of n for various  $\epsilon$ ; values below unity indicate sub-affine deformation. (b) The mean segmental stretch S(n) relative to full extension. (c) The fraction of "highly stretched segments"  $F_{hs}(n)$  as defined in the text with  $S_{min} = 0.7$ . In panel (c) at  $\epsilon = 0.5$ , due to the relatively high level of coarse-graining, the HBD model only predicts a single non-zero point,  $F_{hs} = 4.0 \times 10^{-4}$  for n = 18 Kuhn steps, which is located outside the range of the plot. However, this value is still consistent with that from MD, i.e.,  $F_{hs} = 3.4 \times 10^{-4}$  at n = 18 Kuhn steps.

Kinks. We note in Fig. 1 the appearance of "kinks" or folds, i.e., highly stretched and oriented pairs of adjacent springs with a folded shape as denoted by red springs in Fig. 1(b) at large deformations. Since these "kinks" are localized, as shown below, their frequency is sensitive to the resolution of the HBD model and to the rejuvenation parameter  $\mu$ , unlike the results in Fig. 2. Since the strain hardening behavior of the HBD model is relatively insensitive to both  $\mu$  and to chain resolution (as we will show below; cf. Fig. 5), we anticipate that these kinks do not strongly influence strain hardening for strains that are experimentally attainable for glassy polymers ( $\epsilon < \sim 2$ ). (Localized

kinks do however seem to be important in the evolution of stress in molten polymers at high strain  $(\epsilon > 3)$  and high strain rate.<sup>55</sup>) We identify kinks in both MDCG and HBD chains using coarse-grained vectors that are compatible with the level of resolution in these models; a detailed description of our method is given in the SI. The average numbers of kinks per chain,  $N_{kink}(\epsilon)$ , thereby obtained as functions of the imposed strain for MDCG and HBD conformations are shown in Fig. 3(a) and (c) with three different values of  $N_{HBD}$  and three different values of the rejuvenation parameter  $\mu$ . Unlike the properties plotted in Fig. 3(b) and (d),  $N_{kink}(\epsilon)$  is sensitive to both  $N_{HBD}$  and  $\mu$ ; it is, however, quite insensitive to the uniaxial strain rate in both MD and HBD simulations.  $N_{kink}(\epsilon)$  is strongly dependent on deformation type; for example, it is far lower in uniaxial compression because the direction of chain stretching is perpendicular rather than parallel to the direction of applied strain; see Fig. S11 in the SI.

For each  $N_{HBD}$ , there is a value of  $\mu$  that gives a match between  $N_{kink}(\epsilon)$  predicted by the HBD model and the MD simulations, where the MD configurations have been mapped into the same number of "MDCG" vectors as the number of springs in the HBD model. The best match with the MD results is obtained roughly when the product  $\mu N_{HBD} \cong 2800$ ; see Fig. 3(c) and Fig. 4(a). Since  $\mu$  controls the rate of rejuvenation, the results suggest an interesting coupling between the rate of rejuvenation used in the model for the segmental glassy mode and the degree of coarse-graining used for the polymeric mode. A high value of  $\mu$  means faster mechanical rejuvenation, leading to a faster relaxation of local segmental modes. A sensitivity of kink formation to this value is explained by its effect on local motion and the locking of two neighboring segments into a kink that is not easily unfolded. Increasing  $\mu$  makes unraveling the kink easier, and this is counter-acted by a smaller value of  $N_{HBD}$  which allows more kinks to form, since there are more possible kink

locations when the chain has more beads. Thus, while the stretching of strands of various length is insensitive to coarse-graining, as shown in Fig. 2, accurate a priori resolution of numbers of kinks evidently requires a chain resolved at the monomer or Kuhn step level. Nevertheless, our coarse-grained HBD model can be tuned to produce the same  $N_{kink}(\epsilon)$  as obtained by our fine-grained MD model by setting  $\mu N_{HBD} \cong 2800$ .

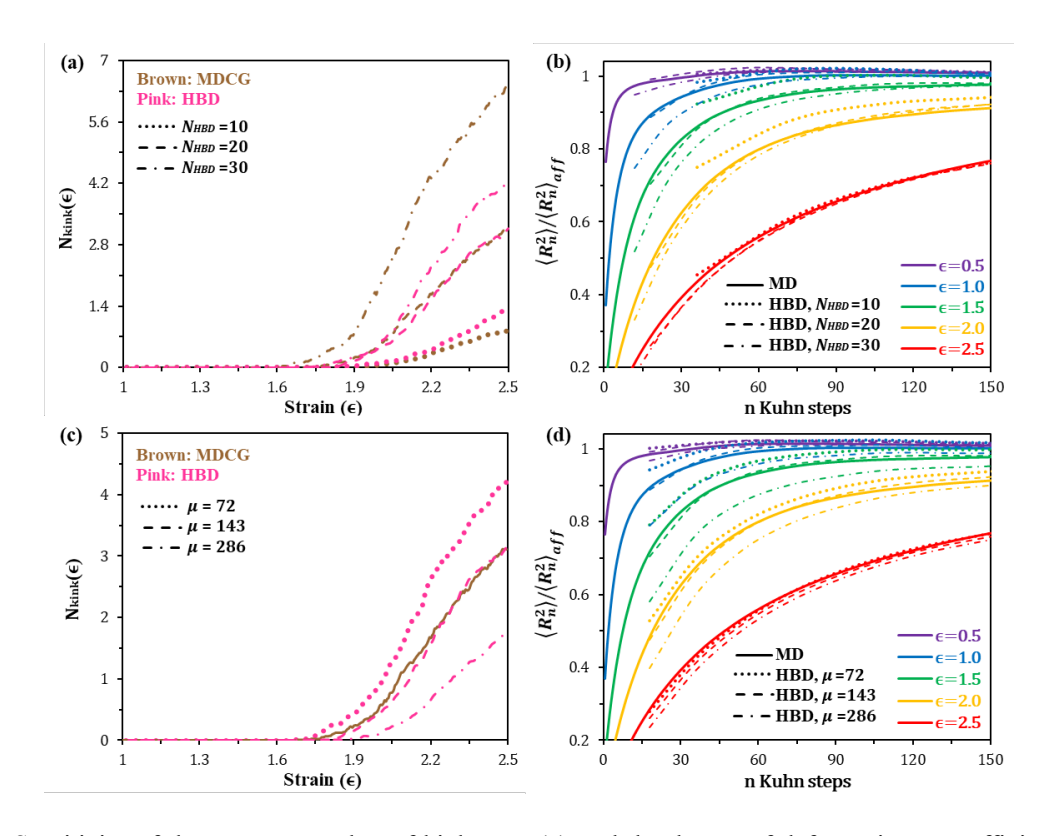


Figure 3. Sensitivity of the average number of kinks  $N_{kink}(\epsilon)$  and the degree of deformation non-affinity for HBD model to the level of coarse-graining  $N_{HBD}$  and rejuvenation parameter  $\mu$ . In (a), numbers of kinks are shown for different levels of coarse-graining of both MDCG model and the HBD model with  $\mu = 143$ . In (c) the effect of the rejuvenation parameter  $\mu$  on  $N_{kink}(\epsilon)$  in the HBD with  $N_{HBD} = 20$  (colored broken lines) is compared to  $N_{kink}(\epsilon)$  in the MDCG model with  $N_{MDCG} = 20$  (thick grey line). In (b) the non-affinity parameter is compared between the MD model (without coarse graining) and the HBD model with  $\mu = 143$  at different levels of coarse-graining, while in (d), a similar comparison is made but with different values of  $\mu$  in the HBD with  $N_{HBD} = 20$ .

Figure 4(a) shows  $N_{kink}(\epsilon)$  determined in the MDCG and HBD models at different levels of coarse-graining. Since many of these kinks will be located in the middle of the coarse-grained MDCG vectors, rather than near their end points, where they can form a kink, the coarse-grained chains in the MDCG model are likely to miss many of them. We therefore identify in Fig. 4(b) the kinks derived from the original (i.e., un-coarse-grained) MD chains. A fold involving only two neighboring bonds of the original MD chain cannot be regarded as a "kink," but we instead require that an abrupt change in chain orientation must persist over multiple original MD bonds for a "kink" to be present. Therefore we choose *any* of the  $N_{MD}$  beads of the original chain as a putative kink position, and draw vectors from this bead's position to the positions of the two beads that lie a chemical distance  $N_{conn}$  away along the chain contour. While in the MDCG chains only MD beads that lie at the ends of the MDCG vectors are candidates to be "kinks," any bead can be recognized as a kink in the original chain. Hence, using the original MD chain, we identify more kinks than in either the MDCG or HBD models, as can be seen in Fig. 4(b).

The results from all three models, (HBD, MDCG, and MD) show that kinks first emerge at a strain that increases from  $\sim 0.5$  to  $\sim 1.2$  as the level of coarse graining increases. For  $\epsilon > \sim 2$ , the MD results in Fig. 4(b) show that  $N_{kink}(\epsilon)$  reaches a plateau, suggesting the system is approaching a limit in which nearly fully stretched and oriented strands are linked by kinks. Beyond this point, chain deformation is dominated by the unraveling of the kinks, if sample failure does not intervene first. Unraveling of the kinked state is seen in melts at high strains  $\epsilon > 3.55,56$  In glassy polymers, however, the stresses become so high that fracture occurs before the kinked state is reached. The smaller  $N_{kink}(\epsilon)$  in the coarse-grained MD and HBD simulations of Fig. 4(a) relative to that for fine-grained MD in 4(b) (where the reader should note the different scales on the y axes of Figs.

4(a) and 4(b)), shows that some conformational details, in particular the full  $N_{kink}(\epsilon)$  have been lost through coarse-graining.

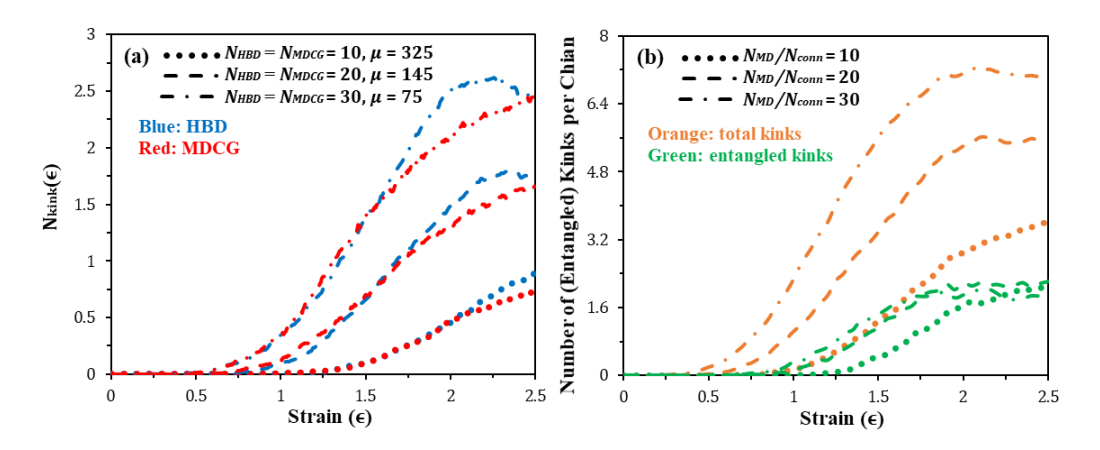


Figure 4. (a) Average numbers of kinks per chain  $N_{kink}(\epsilon)$  as a function of imposed strain for MDCG and HBD models with different levels of coarse-graining. The values of the other parameters are the same as shown in Table I. Note that the values of  $\mu$  are chosen to give the best match of the HBD model to the corresponding MDCG model for the predicted  $N_{kink}(\epsilon)$ . (b) The total number of kinks per chain vs entangled ones as a function of imposed strain in MD simulations. Here, the chains are not coarse-grained into MDCG vectors, but instead two vectors each encompassing  $N_{conn}$  bonds in each of the two directions along the chain are constructed starting at each bead of the original MD chain. The values of  $N_{conn}$  are taken so that  $N_{MD}/N_{conn}$  matches the values of resolution  $N_{MDCG} = N_{HBD} = 10$ , 20, 30 used in the coarse-grained HBD and MDCG models.

Entangled Kinks. To investigate the possible role of entanglements in highly strained glassy polymers, we wish as a first step to find which of the kinks that form in the MD simulations can be considered "entangled." Here, our objective is to identify the entanglements that are localized at kinks since these entanglements most clearly restrict chain motion under deformation. Two kinks are counted as entangled when they lie within a specific distance of each other, belong to different chains, and mutually interwind; the details of how we identify these "entangled kink

pairs" are given in the SI. Of these kinks in Fig. 4(b), we find that a fraction ( $\sim 1/3$ ) can be identified as entangled kinks. While we here find little evidence that either unentangled or entangled kinks influence strain hardening, our method of identifying these entangled kinks in MD simulations could be of use in any future simulations that check for their role in the glassy dynamics of stiffer polymers, or in the crazing regime, where these entangled kinks may be critical in sustaining the integrity of the sample against fracture.

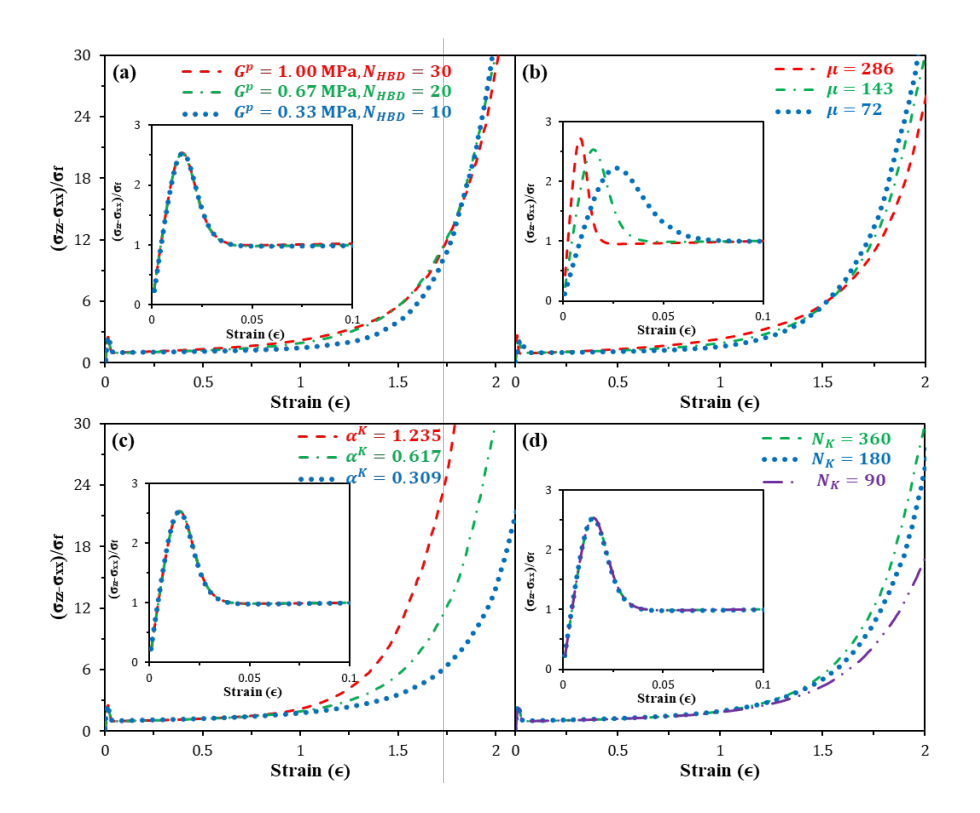


Figure 5. Stress strain behaviors of uniaxial extension predicted by the 1-mode HBD model by varying (a) the level of coarse-graining  $N_{HBD}$  with the modulus of polymeric modes  $G^p$  adjusted accordingly as indicated by Eq. (S4) in the SI; (b) the rejuvenation coefficient  $\mu$ ; (c) the Kuhn length friction ratio  $\alpha^K$ ; and (d) the number of Kuhn steps  $N_K$ . Note that the effects of  $\alpha^K$  and  $N_K$  are accounted by the HBD model through the ratio of polymeric to segmental relaxation times, i.e.,  $\alpha \equiv \alpha^K N_K^2$  as well as the spring constant  $N_{K,s}$ . In the above four panels, the tensile stress is normalized by the corresponding flow stress defined at strain  $\epsilon = 0.1$ , and all the adjustable parameters are kept at the same values as those in Table I unless stated otherwise. The inserts are blow-ups of the normalized stress in the small-strain region.

Strain Hardening. We plot in Fig. 5 the stress predicted by the 1-mode HBD model for various values of model parameters, including resolution  $N_{HBD}$ , rejuvenation parameter  $\mu$ , polymer relaxation parameter  $\alpha^{K}$ , and length of chain in number of Kuhn steps  $N_{K}$ . The hardening behavior is relatively insensitive to the level of coarse graining  $N_{HBD}$  of the model, as shown in Fig. 5(a), where the definition of polymer modulus  $G^p$  makes it vary inversely related to  $N_{HBD}$  (see SI for details). Similarly, Fig. 5(b) shows that while the rejuvenation parameter  $\mu$  strongly influences the elastic modulus, yield stress and yield strain, it has a relatively small effect on the degree of strain hardening when it is normalized by the flow stress. We note that both the flow stress and the hardening modulus are inversely proportional to  $\mu$ . As discussed earlier,  $\alpha \equiv \tau^p/\tau^s = \alpha^K N_K^2$  is controlled by the chain length  $N_K$  and by the ratio  $\alpha^K = \tau^K/\tau^s$  of the Kuhn step relaxation time to the segmental relaxation time, the latter of which is set by the glassy mode in the HBD model. Fig. 5(c) shows that at fixed  $N_K$  the degree of strain hardening increases rapidly with increasing  $\alpha^K$ . This behavior is consistent with our suggestion that  $\alpha^{K}$  is a measure of the effect of chain stiffness on polymer relaxation time. However, the  $\alpha^{K}$ -independence of the stress-strain curves for  $\epsilon < \sim 0.8$ indicates that the parameter  $\alpha^{K}$  does not by itself capture all chain-stiffness effects; in real systems, stiffer chains produce larger  $F(\epsilon)$  at far smaller strains.<sup>22,34</sup> Figure 5(d) illustrates the effect of varying  $N_K$  with  $\mu$  and  $\alpha^K$  fixed. The increase in hardening with increasing chain length is consistent with both experiments<sup>57</sup> and simulations.<sup>25,27</sup> Note that while the onset strains for kink formation in Fig. 4(a) correspond roughly with the onset strains for strain hardening for each of these levels of resolution, as shown in Fig. 5(a) below, the strong dependence of  $N_{kink}(\epsilon)$  on the level of coarsegraining for higher strains in Fig. 4(a) is not reflected in the stress-strain curves. Therefore we do not believe that kinks, entangled or otherwise, are a principal cause of glassy strain hardening.

Yielding. The inserts to Fig. 5 show that the behavior of the 1-mode HBD model in the vicinity of the yield point is unrealistic, with an abnormally large stress overshoot. This unrealistic behavior becomes even more obvious when the strain rate is varied, as shown in Fig. 6. While for the lowest strain rate in Fig. 6(b) the magnitude of the overshoot predicted by the HBD model is comparable to that for the MD simulation at its lowest strain rate, the overshoot in the HBD model grows rapidly with increasing strain rate and quickly becomes unrealistically high. The overshoot at any one strain rate can be corrected by adjustment of parameters, but this leads to failure when the strain rate is varied. Note that in Fig. 6 the flow stress  $σ_f$  used to normalize the y axis is that for the intermediate strain rate, while in Fig. 5 each curve is normalized by its own flow stress. This allows the effect of strain rate on flow stress to be revealed in Fig. 6. Experiments and MD simulations show that  $σ_f$ , is roughly logarithmic in strain rate (insert to Fig. 6(a)), while the fluidity model shows little dependence of flow stress on strain rate if the strain rate is higher than the inverse of the waiting time (see the insert to Fig. 6(b)). Thus, the fluidity model gives far too strong a dependence of stress overshoot on strain rate, but too weak a dependence of flow stress.

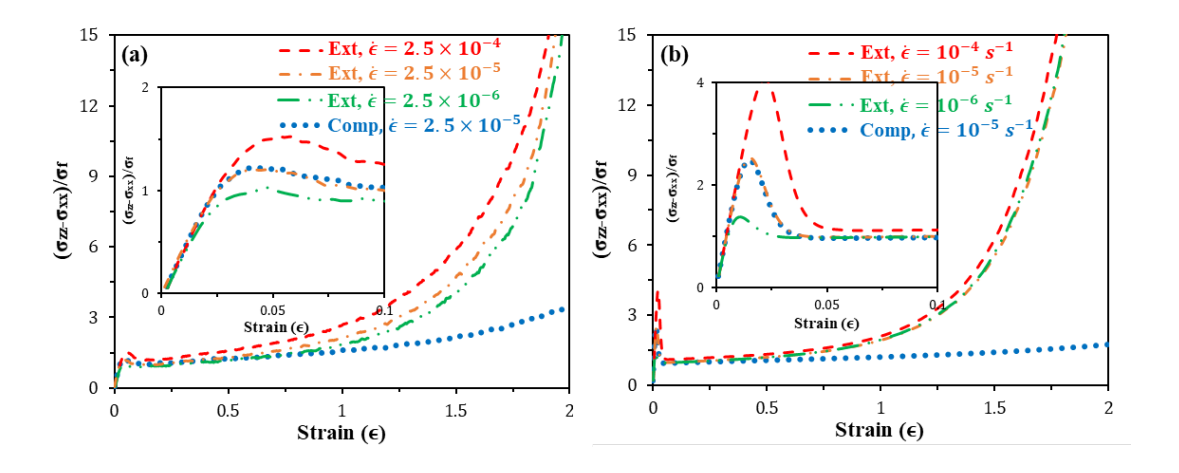


Figure 6. Mechanical responses of uniaxial extension under three different rates as well as compression predicted from (a) the fine-grained Kremer-Grest polymer model and the coarse-grained HBD model with (b) 1-mode segmental relaxation, where the segmental mode dynamics are computed from Eqs. (1a) and (1b). The stress in the above panels is normalized by the flow stress at the intermediate strain rate, i.e.,  $\dot{\epsilon} = 2.5 \times 10^{-5}$  (in LJ units) for MD and  $\dot{\epsilon} = 10^{-5}$  s<sup>-1</sup> for HBD, which yields (a)  $\sigma_f = 0.854$  in LJ units of  $u_0/a^3$ , and (b)  $\sigma_f = 6.18$  MPa. The inserts are blow-ups of the normalized stress in the small-strain region. For these predictions, we took  $G^s = 480$  MPa and  $t_w = 8.3$  h.

This failure of the simple 1-mode HBD model to predict the behavior near yield does not seem to greatly influence its predictions for the strain hardening regime, which are in semi-quantitative agreement with the MD results. Thus, as the strain hardening region is entered, polymer stretching and stress are evidently rather insensitive not only to polymer coarse graining (as revealed in Fig. 2), but also to the details of the segmental dynamics, e.g. the presence or absence of a broad distribution of segmental relaxation times. This is consistent with previous results which have shown that segment-scale relaxation becomes more homogeneous in the strain-hardening regime.<sup>58</sup> The response near the yield strain, however, is very sensitive to the segmental model. Figure 6(b) shows that the 1-mode HBD model severely overpredicts the degree of post yield strain softening seen in the MD simulations. This indicates that the near-universal behavior of the nonaffinity, stretch, and fraction of highly stretched strands illustrated in Fig. 2 does not extend to the stress-strain behavior near the yield point, which is much more sensitive to the dynamics of the segmental mode. The results in Fig. 6 reinforce our claim that strain hardening is controlled primarily by chain stretching (at various length scales down to sub-entangled ones), and is tightly coupled to the glassy segment-scale dynamics. They also demonstrate that our simple single-chainin-mean-field model without explicit entanglements can at least qualitatively capture even dramatic strain hardening, although failing badly to predict behavior near the yield point.

The Origin of Strain Hardening in Glassy Polymers. The strain hardening observed in crosslinked rubbers is entanglement- and crosslink-driven at modest Weissenberg numbers because subentangled chain segments relax rapidly compared to the inverse strain rate. In glasses, this is no longer the case, since even the post-yield Weissenberg number Wip is typically high; in both our MD and HBD simulations it is  $Wi^p \sim 10^3$ . Here we have defined  $Wi^p = \tau^p \dot{\epsilon} = \alpha \tau_{ss}^s \dot{\epsilon}$ , where  $\tau_{ss}^s$  is the steady state value of the segmental relaxation time. (It has been shown by fluorescence spectroscopy 59-62 that the segmental relaxation time usually approaches a plateau value  $au_{ss}^s(\dot{\epsilon})$  at strains beyond the yield strain for uniaxial extension at constant  $\dot{\epsilon}$ .) By solving Eq. 1 at steady state, we obtain  $Wi^p = \alpha/(\sqrt{3}\mu) = 323$ , which in our model is independent of strain rate, but in a real glass should increase logarithmically with strain rate. At such high Wip, we have seen that the highly stretched strands discussed above first begin to appear at a strain of  $\epsilon \sim 0.5$ , and become increasingly prominent as stress and strain increase, especially for  $\epsilon > 1.0$  Strain hardening in polymer glasses does not require fully formed folded kinks, 55 but only their precursors, the highly stretched strands. Note also that since  $\alpha \propto N_K^2$ , decreasing the chain length decreases the Weissenberg number. As Wip decreases, the glassy polymer acts more like a melt, and strain hardening weakens (and is delayed). The predicted gradual decrease in strain hardening as  $N_K$ decreases — or equivalently, saturation of strain hardening as  $N_K$  increases — shown in Fig. 5(d) is consistent with results from MD simulations. 25,27

Previous studies<sup>26,28</sup> have noted that polymer chain connectivity and uncrossability *require* polymer glasses to deform plastically on length scales over which chains deform subaffinely, and postulated that the increasingly subaffine deformation as strain increases drives the dominant

dissipative component of strain hardening. Our results extend this picture by making the role played by strand-stretching much more explicit and by showing that the subaffine deformation and strand-stretching are nearly quantitatively captured by our single-chain-in-mean-field model. Both MD and HBD simulations show that the characteristic subaffine-affine crossover chemical distance  $(n^*)$  increases with strain. Larger plastic events have larger activation energies (i.e. require more work to activate), which means that stress *must* increase with strain. Our results clarify that the reason entanglements are not primary in this picture is that the chemical length scale controlling the onset of strain hardening  $(n^*)$  remains below the rheological entanglement length  $N_e$ . Our observation (in Fig. 2(a)) of  $n^* \sim N_e/3$  in the early stages of strain hardening is consistent with the earlier observation<sup>30</sup> that the length scale over which strands are pulled taut in stable crazes is  $\sim N_e/3$  rather than  $\sim N_e$ . While Kramer concluded long ago that experimental results for strain hardening over a wide range of temperatures in systems with a wide range of entanglement densities dictate  $n^* < N_e$ , 20 the underlying microscopic phenomenology has not heretofore been made so specific. Note that we do not claim that strong strain hardening can occur in experiments on unentangled systems — it is now well established that an entanglement network is required to prevent brittle fracture before the onset of strain hardening. 15,17,22,47

Since HBD uses a very simplistic model for the glassy segmental mode (that is coupled to the polymeric mode only through a friction coefficient), while the MD simulations are resolved at or below the level of the segmental mode, the good agreement between the two models in both their chain configurations shown in Fig. 2 and in their strain hardening in Figs. 5 and 6 is strong evidence that the polymer configurations and strain hardening are not sensitive to the finer details of the glassy dynamics. In addition, the insensitivity of the results to the inclusion of entanglements

(which are present in the MD simulations but not in the HBD simulations) provides further evidence that the polymeric modes in deformed glasses — at least for highly flexible polymers — can be modeled using simple bead-spring chains without explicit entanglements. On the other hand, the segment-scale model used above is clearly inadequate for prediction of yielding and strain softening. Furthermore, although the hardening stress  $\sigma_f[F(\epsilon)-1]$  arises largely from the highly stretched strands as detailed above, it is ultimately governed by the friction exerted on those strands by surrounding segments, and this friction in turn depends strongly on the glassy modes. Therefore we now turn our attention to developing a better segment-scale model.

Improved. The above successes of our simplified modeling, in particular in the agreement of MD and HBD simulations of chain configurations shown in Fig. 1 and quantified in Fig. 2, and the hardening in Figs. 5 and 6 does not carry over to the prediction of yielding behavior. (For additional details, see "Drawbacks of single-mode segmental model" in the SI for details.) This is both because the rejuvenation model is overly simplified and because use of a single relaxation time ignores the heterogeneity of the segmental dynamics, whose rates of molecular rearrangements vary significantly across spatial and temporal scales. 59-62.65 Thus, we need improvements in our description of the dynamics at the segmental level to include, at the least, the effects of stretched exponential relaxation (known as the Kohlrausch-Williams-Watts, or KWW function) on the nonlinear deformation behaviors, especially for loading and unloading. We believe that this could be achieved by employing multiple segmental relaxation times (as opposed to the single one assumed previously) within the abovementioned "glassy solvent" description of segmental dynamics. Since the characteristic probe relaxation time  $\tau_{prb}^{s}$  and the stretching exponent  $\beta$  of a

KWW function has been accurately measured by fluorescence spectroscopy at each instant deformation time,  $^{59-62}$  we here construct a small set of distinct Maxwell modes from the decomposition of these KWW functions into a discrete spectrum of Maxwell time constants with the corresponding amplitude of each mode tuned iteratively at given  $\tau^s_{prb}$  and  $\beta$ . In this way, we extend the single-mode segmental dynamics in the original HBD model,  $^{45}$  whose relaxation time is governed by the fluidity equation, to a discrete spectrum of modes with relaxation times derived from the decomposition of the stretched exponential function at given  $\tau^s_{prb}$  and  $\beta$ , i.e.,

$$\begin{cases}
\dot{\boldsymbol{\sigma}}_{j}^{S} + \boldsymbol{v} \cdot \nabla \boldsymbol{\sigma}_{j}^{S} = \boldsymbol{\sigma}_{j}^{S} \cdot \nabla \boldsymbol{v} + (\nabla \boldsymbol{v})^{T} \cdot \boldsymbol{\sigma}_{j}^{S} - (\boldsymbol{\sigma}_{j}^{S} - \boldsymbol{I})/\tau_{j}^{S} \\
\boldsymbol{\Sigma}^{S} = G^{S} \sum_{j}^{M} C_{j} (\boldsymbol{\sigma}_{j}^{S} - \boldsymbol{I})
\end{cases} (2a)$$

$$\begin{cases}
exp\left[-\left(\frac{x}{\tau_{prb}^{s}}\right)^{\beta}\right] = \sum_{j}^{M} C_{j} exp\left(-\frac{x}{\tau_{j}^{s}}\right) \\
\frac{\tau^{p}}{\sum_{j}^{M} C_{j} \tau_{j}^{s}} = \alpha, \tau_{prb}^{s}\big|_{t=0} = t_{w}
\end{cases} (2b)$$

In the above,  $\sigma_j^s$  stands for the segmental configuration tensor for mode j with the corresponding amplitude  $C_j$  and characteristic time  $\tau_j^s$  determined by a genetic algorithm, whose details are given in the SI. M=3 is the total number of segmental modes used here to represent the KWW function with experimental determined *time-dependent*  $\tau_{prb}^s$  and  $\beta$ . This means that  $C_j$  and  $\tau_j^s$  are also time dependent, and in a properly invariant constitutive equation would need to be rendered functions of one or more internal variables, or by using strain history integrals, as have been developed in the literature. We leave them as functions of time to illustrate how better stress predictions might be made possible by improving the model of the glassy mode. We note that similar predictions could be made, up to the yield point, by making them functions of segmental stress

rather than time. The glassy and polymeric configuration tensors  $\sigma_j^{p,s}$  contribute to the stress ( $\Sigma^{p,s}$ ) through their moduli  $G^{p,s}$ , where the polymeric stress tensor is obtained from the forces and configurations of the HBD springs, using the standard Kramers formula as discussed in our earlier work.<sup>30</sup> The waiting time  $t_w$  is controlled by how long the sample has been aged since the last deformation. Thus, assuming that rejuvenation remains governed by the deformation-rate-dependent fluidity equation (Eq. (1)), the values of  $G^s$  and  $f_w$  are obtained in this new version of the model by fits to the experimental stress-strain curve using  $f_{prb}^s$  and  $f_w$  directly measured from fluorescence spectroscopy.

Note that the above multimode Maxwell model with time-dependent relaxation times only accounts for spatial heterogeneity at a mean-field level: namely, only to the extent that the decomposed stretched exponential represents an average of the segmental relaxation function over the spatial distribution of microdomains. In addition, we do not attempt here to develop a properly invariant full constitutive model for segmental relaxation. Instead we employ experimental segmental-relaxation data for a specific strain history and attempt to predict its effects on polymer relaxation and stress strain curves *for the same strain history*. The time-dependence of the relaxation times and moduli would be different for other strain histories and could only be obtained by measurements in those histories. In fact, since we continue to use the overly simple rejuvenation model in Eq. (1), the revised segmental model, *with parameters from an experiment at one particular strain rate*, will not properly capture the strain rate dependence of stress near the yield point at other strain rates. However, since the time dependence of the segmental relaxation spectrum must in any event be obtained experimentally, there is no use repairing the rejuvenation model until a proper complete constitutive equation for the relaxation time spectrum is developed.

Ultimately, it will be necessary to develop a proper constitutive equation for the segmental mode that can predict these segmental relaxation dynamics for arbitrary deformation histories, and combine this with our polymeric model to obtain a full constitutive model of the polymer glass. For now, however, our goal is limited to checking the extent to which a more accurate accounting of the segmental dynamics (obtained from the experimental data), when coupled with our model of the polymeric mode, is able to improve predictions of the strain hardening phenomenon.

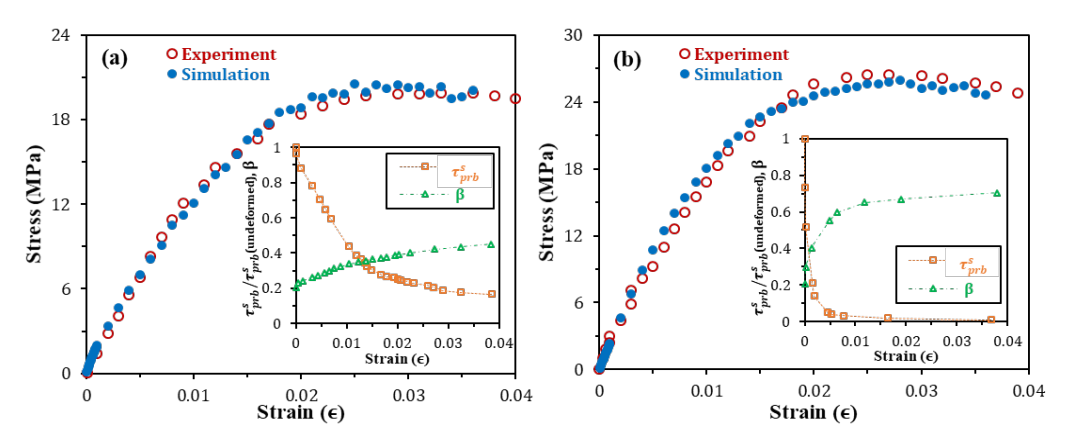


Figure 7. Comparison of HBD simulation results predicted by the empirical 3-mode segmental model with parameters given in Table I (except using a shorter initial age of the glass  $t_w$  and a larger glassy modulus  $G^s$  given below) with stress-strain curves of Ediger and coworkers<sup>59-62</sup> under steady uniaxial extensional straining of PMMA at 373 K with (a)  $\dot{\epsilon} = 1.5 \times 10^{-6} \text{ s}^{-1}$  and (b)  $\dot{\epsilon} = 3.1 \times 10^{-5} \text{ s}^{-1}$ . The time-dependent probe segmental relaxation time  $\tau_{prb}^s$  and stretched exponential exponent  $\beta$  taken from their smoothed fluorescence spectroscopy data are shown in the inserted plots. To be consistent with the experimental results in references, <sup>59-62</sup> the strain along the horizontal axis is taken as the global strain, but the simulations used the actual strain measured near the mid-point of the sample where segmental relaxation was measured. The fitting values are (a)  $G^s = 900 \text{ MPa}$ ,  $t_w = 3.3 \text{ h}$  for  $\dot{\epsilon} = 1.5 \times 10^{-6} \text{ s}^{-1}$ ; and (b)  $G^s = 800 \text{ MPa}$ ,  $t_w = 5.8 \text{ h}$  for  $\dot{\epsilon} = 3.1 \times 10^{-5} \text{ s}^{-1}$ , semi-quantitatively reflecting the effects of temperature and preparation history of the testing samples. Only values of parameters relevant to the glassy mode are important at the low strains.

As illustrated in Fig. 7, we performed HBD simulations using this new modified segmental model based on experimental data points for  $\tau^s_{prb}$  and  $\beta$ , and obtained good agreement with the experimental stress at the beginning of startup flow. Note that since the final strains considered in Fig. 7 are still in the pre-strain-hardening regime, the predicted mechanical responses are dominated by the segmental dynamics with insignificant contributions from the polymeric mode, where both  $\tau_{prb}^{s}$  and  $\beta$  in Eq. (2) are obtained experimentally without using the simple fluidity equation in Eq. (1). Therefore, the only relevant parameters (among all the others shown in Table I) are  $t_w$  and  $G^s$ , which can be estimated directly by matching the simulation predictions with the data from experiments. The agreement shown in Fig. 7 is much better than we can obtain with onemode models; Fig. S12 shows that the latter produce much stronger strain-softening, whether the single relaxation time is obtained from the fluidity model or directly from the experimental data. We also find that the corresponding best-fit values of both  $t_w$  and  $G^s$  (Table S1 in SI) deviate from ranges that reflect the physical properties of a young glass. These results all indicate the importance of a multi-mode description for development of a physics-based segmental relaxation model. Finally, we found that the 3-mode model can predict stress-strain curves near the yielding region that much better match those obtained the MD simulations (and experiments). Although not shown here, the hardening behavior predicted by the 3-mode segmental model is very similar to that predicted by the simple 1-mode model, as expected. This is not surprising, since we have shown that the hardening modulus, when normalized by the flow stress, is insensitive to the segmental model.

Much progress has been made recently in understanding segmental-level dynamics of both small-molecule and polymeric glasses.<sup>67-69</sup> However, segment-scale theories such as the PNLE theory of

Schweizer et al. 38-41 typically do not treat polymeric relaxation modes; indeed they typically assume chains deform affinely above segmental scales. Efforts to obtain improved predictions of glassy-polymeric mechanical response should therefore combine the most recent and most accurate treatments of segment-scale physics with the larger-scale polymer physics described here — in particular, the formation of highly stretched segments. A very useful future direction would be to capture thermo-mechanical effects in an accurate model of the glassy mode, and combine this with the description of the polymer mode described here to provide improved understanding of the effects of thermomechanical history on the stress-strain properties of glassy polymers. It will also be important to determine if entangled or untangled "kinks," which require fine-grained modeling to capture accurately, are important in determining properties of the yielded glass, such as birefringence, thermomechanical history, and breakage stress. For example, it is quite likely that entangled kinks will become important in the dramatic hardening regime where increasing strand tension increases the energetic component of stress. <sup>26,28</sup> We hope that the findings presented here will help the community achieve a useful synthesis of these ideas and hence a more complete understanding of polymeric glasses and their rheology, as well as some directions for further research.

## **Summary and Future Directions**

Analyses at two different levels of resolution have provided insight into the effect of multiple segmental relaxation times and sub-entanglement chain stretching on strain hardening and stress-strain relationships in tensile deformations of polymeric glasses. Both our HBD model and the finer-grained MD simulations suggest that sub-entanglement chain stretching and orientation

trigger strain-hardening in polymeric glasses at a strain level ( $\epsilon \sim 1$ ) that is much smaller than would be required if strain-hardening originated from the affine deformation of an entangled network. MD simulations clearly exhibit the emergence of highly-stretched segments with chain conformations very similar to those found in HBD simulations, and indicating that strain hardening is controlled primarily by chain stretching at high Weissenberg number, and not by entanglements or details of the glassy dynamics. This similarity of results from both fine-grained and coarse-grained models offers a clear explanation of the large magnitude of glassy-polymer strain-hardening: hardening in the glassy state arises primarily from chain stretching and orientation at scales below that of the entanglement mesh. This picture supports the notion<sup>26</sup> that while entanglements are essential for stabilizing glassy polymers against brittle fracture, they are of less importance in strain hardening itself.

The successful prediction of chain stretching and strain hardening from our original coarse-grained model does not extend to the yielding behavior, which requires a more accurate description of the glassy mode than is provided in our original very simple one-mode fluidity model. We therefore further modified our model by extending the segmental relaxation from one mode to three modes whose dynamics were drawn from experimental measurements, namely the time-dependent values of segmental relaxation time  $\tau_{prb}^s$  and stretching exponent  $\beta$  probed by fluorescence spectroscopy on deforming polymeric glasses. With this revised segmental model, we observed much better predictions in pre-yield and yielding regimes where the segmental mode contributes most of the stress and where overshoot occurs. The new three-mode HBD model implicitly accounts for local heterogeneity to the extent that it can be represented by stretched exponential relaxation. The success of this more accurate segmental model, however, depends on having measured data on

segmental relaxation for each strain history. Thus, the model only allows good predictions of stress in the region of yield if accurate segmental relaxation times are available from experiments. Future work should endeavor to develop a robust segmental constitutive model that accurately predicts the experimental segmental relaxation in arbitrary strain histories and incorporates this into HBD simulations to get a complete depiction for polymer glasses under deformation. Testing multimode HBD theory against MD simulations of glasses deformed well into the strain-hardening regime, over a wide range of temperatures, for a wide range of chain stiffnesses should be particularly useful in this effort because MD simulations allow for far more precise characterization<sup>48,58</sup> of multiscale structural relaxation than is currently achievable experimentally. For example, comparing results for different chain stiffnesses will allow our hypotheses about the effect of stiffness on the Kuhn-level friction parameter  $\alpha^{\kappa}$  to be directly tested.

Thus, while the work reported here leaves much left to do, it does provide some clear conclusions about the source of strain hardening. It also provides a starting point for further work on developing a constitutive theory that covers both plastic flow and hardening, as well as methods for analyzing the role of entanglements near the onset of failure.

# Acknowledgements

The authors acknowledge support from the National Science Foundation (NSF) under grants DMR-1403335, DMR-1707640, and DMR-1555242. Any opinions, findings, and conclusions or recommendations expressed in this material are those of the authors and do not necessarily reflect the views of NSF.

## **Supporting Information**

The Supporting Information contains the following information. First, we discuss how the level of coarse-graining affects the choice of parameters, including, in particular the polymer modulus  $G^p$  and rejuvenation parameter  $\mu$ . Next we demonstrate that chain conformations during deformation are insensitive to the level of coarse-graining and to the rejuvenation parameter  $\mu$ . Then we show that chain conformations predicted by the HBD model match those of the MD model over a wide range of extension rates, and also for compressive deformation. Then we describe our method for identifying kinks and entangled kink pairs; we also discuss the sensitivity of the number of kinks to the details of the kink-identification criteria, such the kink angle and the stretch of segments adjacent to the kink. Then we discuss the drawbacks of the single-mode segmental model, and illustrate the need for our "three-mode model." Then we describe our method for converting the stretched exponential KWW function [Eq. 2(b)] into a three-model model wherein the relaxation times and relaxation amplitudes of the three modes as a function of time are derived from the experimental data for the (time-dependent)  $\tau_{prb}^s$  and  $\beta$ . Finally we demonstrate a correlation between segmental mobility and  $\beta$  that is derived from experimental data.

#### Reference

- [1] Cubuk, E. D.; Ivancic, R. J. S.; Schoenholz, S. S.; *et al.* Structure-property relationships from universal signatures of plasticity in disordered solids. *Science* **2017**, *358*, 1033–1037.
- [2] Zhang, K.; Meng, D.; Müller-Plathe, F.; Kumar, S. K. Coarse-grained molecular dynamics simulation of activated penetrant transport in glassy polymers. *Soft Matter* **2018**, *14*, 440–447.
- [3] Zhang, W.; Douglas, J. F.; and Starr F. W. Dynamical heterogeneity in a vapor-deposited polymer glass. *J. Chem. Phys.* **2017**, *146*, 203310.
- [4] Morgan, R. J.; and O'neal J. E. The mechanical properties of polymer glasses. *Polymer-Plast. Technol. Eng.* **1975**, 5, 173-197.
- [5] Phillips, J. C. Microscopic aspects of Stretched Exponential Relaxation (SER) in homogeneous molecular and network glasses and polymers. *J. Non-Cryst. Solid.* **2011**, *357*, 3853-3865.
- [6] Zhao, Y.; Liu, J.; Li, X.; *et al.* How and why polymer glasses lose their ductility due to plasticizers. *Macromolecules* **2017**, *50*, 2024-2032.
- [7] Ge, T.; Tzoumanekas, C.; Anogiannakis, S. D.; *et al.* Entanglements in glassy polymer crazing: cross-links or tubes? *Macromolecules* **2017**, *50*, 459-471.
- [8] Hebert, K.; and Ediger, M. D. Reversing strain deformation probes mechanisms for enhanced segmental mobility of polymer glasses *Macromolecules* **2017**, *50*, 1016-1026.
- [9] Chung, Y. G.; and Lacks, D. J. Sheared polymer glass and the question of mechanical rejuvenation. *J. Chem. Phys.* **2012**, *136*, 124907.
- [10] Malekmotiei, L.; Voyiadjis, G. Z.; Samadi-Dooki, A.; *et al.* Effect of annealing temperature on interrelation between the microstructural evolution and plastic deformation in polymers. *J. Polym. Sci. B* **2017**, *55*, 1266-1297.
- [11] Xu, W-S.; Douglas, J. F.; and Freed, K. F. Generalized entropy theory of glass-formation in fully flexible polymer melts. *J. Chem. Phys.* **2016**, *145*, 234509.
- [12] Arzhakov, M. S.; Lukovkin, G. M.; and Arzhakov, S. A. Concept of generalized polymer glass. *Dokl. Phys. Chem.* **2002**, *384*, 119-122.
- [13] Hoy, R. S.; Foteinopoulou, K.; Kröger, M. Topological analysis of polymeric melts: Chain-length effects and fast-converging estimators for entanglement length. *Phys. Rev. E* **2009**, *80*, 031803.

- [14] Paeng, K.; Lee, H-N.; Swallen, S. F.; and Ediger, M. D. Temperature-ramping measurement of dye reorientation to probe molecular motion in polymer glasses. *J. Chem. Phys.* **2011**, *134*, 024901.
- [15] Liu, J.; Lin, P.; Li, X.; Wang, S-Q. Nonlinear stress relaxation behavior of ductile polymer glasses from large extension and compression. *Polymer* **2015**, *81*, 129-139.
- [16] Kumar, R.; Goswami, M.; Sumpter, B. G.; *et al.* Effects of backbone rigidity on the local structure and dynamics in polymer melts and glasses. *Phys. Chem. Chem. Phys.* **2013**, *15*, 4604-4609.
- [17] Zartman, G. D.; Cheng, S.; Li, X.; *et al.* How melt-stretching affects mechanical behavior of polymer glasses. *Macromolecules* **2012**, *45*, 6719-6732.
- [18] De Focatiis, D. S. A.; Embery, J.; Buckley, P. Large deformations in oriented polymer glasses: experimental study and a new glass-melt constitutive model. *J. Polym. Sci. B* **2010**, *48*, 1449-1463.
- [19] Chung, Y. G.; and Lacks, D. J. Atomic mobility in a polymer glass after shear and thermal cycles. *J. Phys. Chem. B* **2012**, *116*, 14201-14205.
- [20] Kramer, E. J. Open questions in the physics of deformation of polymer glasses. *J. Polym. Sci. Part B Polym. Phys.* **2005**, *43*, 3369-3371.
- [21] Hsu, H.-P.; and Kremer, K. Primitive path analysis and stress distribution in highly strained macromolecules. *ACS Macro. Lett.* **2018**, *7*, 107-111.
- [22] Kramer, E. J.; Microscopic and molecular fundamentals of crazing. Adv. Polym. Sci. 1983, 52-53, 1.
- [23] Ge, T.; Robbins, M. O. Anisotropic plasticity and chain orientation in polymer glasses. *J. Polym. Sci. B* **2010**, *48*, 1473-1482.
- [24] Hoy. R. S.; and Robbins, M. O.; Strain hardening in bidisperse polymer glasses: Separating the roles of chain orientation and interchain entanglement. *J. Chem. Phys.* **2009**, *131*, 244901.
- [25] Hoy, R. S.; and Robbins. M. O.; Strain Hardening in Polymer Glasses: Limitations of Network Models. *Phys. Rev. Lett.* **2007**, 99, 117801.
- [26] Hoy, R. S.; Why is understanding glassy polymer mechanics so difficult? *J. Polym. Sci. Part B Polym. Phys.* **2011**, *49*, 979-984.
- [27] Hoy, R. S.; and Robbins, M. O.; Strain Hardening of Polymer Glasses: Effect of Entanglement Density, Temperature, and Rate. *J. Polym. Sci Part B Polym. Phys.* **2006**, 44, 3487-3500.

- [28] Hoy, R. S.; and Robbins, M. O.; Strain hardening of polymer glasses: Entanglements, energetics, and plasticity. *Phys. Rev. E* **2008**, *77*, 031801.
- [29] Nguyen, H. T.; and Hoy, R. S.; Effect of the ratio l<sub>k</sub>/p on glassy-polymeric shear deformation mechanisms. *Macromolecules* **2018**, *51*, 4370-80.
- [30] Rottler, J.; and Robbins, M. O.; Growth, microstructure, and failure of crazes in glassy polymers. *Phys. Rev. E* **2003**, *68*, 011801.
- [31] Hasan, O. A; and Boyce, M. C.; Energy storage during inelastic deformation of glassy polymers. *Polymer* **1993**, *34*, 5085.
- [32] Govaert, L. E.; Engels, T. A. P.; Wendlandt, M.; Tervoort, T. A.; and Suter, U. W.; Does the Strain Hardening Modulus of Glassy Polymers Scale with the Flow Stress? *J. Polym. Sci Part B Polym. Phys.* **2008**, 22, 2475-2481.
- [33] Liu, J; Zhao, Z; Wang, W; Mays, J. W.; and Wang, S.-Q.; Brittle-Ductile Transition in Uniaxial Compression of Polymer Glasses. *J. Polym. Sci Part B Polym. Phys.* **2019**, 57, 758-770.
- [34] Haward, R. N.; Strain hardening of thermoplastics. *Macromolecules* **1993**, 26, 5860-69.
- [35] van Melick, H. G. H.; Govaert, L. E. and Meijer, H. E. H. On the origin of strain hardening in glassy polymers. *Polymer* **2003**, 44, 2493-2502.
- [36] Smessaert, A.; Rottler, J. Recovery of polymer glasses from mechanical perturbation. *Macromolecules* **2012**, *45*, 2928-2935.
- [37] van Breemen, L. C. A.; Klompen, E. T. J.; Govaert, L. E.; Meijer, H. E. H. Extending the EGP constitutive model for polymer glasses to multiple relaxation times. *J. Mech. Phys. Solids* **2011**, *59*, 2191-2207.
- [38] Chen, K. and Schweizer, K. S. Theory of aging, rejuvenation, and the nonequilibrium steady state in deformed polymer glasses. *Phys. Rev. E* **2010**, *82*, 041804.
- [39] Chen, K. and Schweizer, K. S. Theory of relaxation and elasticity in polymer glasses. *J. Chem. Phys.* **2007**, *126*, 014904.
- [40] Chen, K; and Schweizer, K. S; Theory of yielding, strain softening, and steady plastic flow in polymer glasses under constant strain rate deformation. *Macromolecules* **2011**, 44, 3988-4000.
- [41] Chen, K.; and Schweizer, K. S.; Molecular theories of segmental dynamics and mechanical response in deeply supercooled polymer melts and glasses. *Ann. Rev. Cond. Matt. Phys.* **2010**, *1*, 277-300.

- [42] Nayak, K.; Read, D. J.; McLeish, T. C. B.; Hine, P. J. Tassieri, M. A coarse-grained molecular model of strain-hardening for polymers in the marginally glassy state. *J. Polym. Sci. Part B Polym. Phys.* **2011**, *49*, 920-938.
- [43] Fielding, S. M.; Larson, R. G.; and Cates, M. E. Simple model for the deformation-induced relaxation of glassy polymers. *Phys. Rev. Lett.* **2012**, *108*, 048301.
- [44] Fielding, S. M.; Moorcroft, R. L.; Larson, R. G.; and Cates, M. E. Modeling the relaxation of polymer glasses under shear and elongational loads. *J. Chem. Phys.* **2013**, *138*, 12A504.
- [45] Zou, W.; and Larson, R. G. A hybrid Brownian Dynamics/constitutive model for yielding, aging, and rejuvenation in deforming polymeric glasses. *Soft Matter* **2016**, *3*, 3853-3865.
- [47] Li, X. X.; Liu, J. N. Liu, Z. N.; Tsige, M.; and Wang, S. Q. Illustrating the molecular origin of mechanical stress in ductile deformation of polymer glasses. *Phys. Rev. Lett.* **2018**, *120*, 077801.
- [48] Rottler, J. Relaxation times in deformed polymer glasses: A comparison between molecular simulation and two theories. *J. Chem. Phys.* **2016**, *145*, 064505.
- [49] Xu, J.; Li, D.; Chen, J.; *et al.* Detection of interchain proximity and segmental motion of polymer glass. *Macromolecules* **2011**, *44*, 7445-7450.
- [50] Riggleman, R. A.; Lee, H-N.; Ediger, M. D. and de Pablo, J. J. Free volume and finite-size effects in a polymer glass under stress. *Phys. Rev. Lett.* **2007**, *99*, 215501.
- [51] Kremer, K; Grest, G. S. Dynamics of entangled linear polymer melts a molecular dynamics simulation. *J. Chem. Phys.* **1990**, *92*, 5057-86.
- [52] Auhl. R.; Everaers, R; Grest, G. S.; Kremer, K; and Plimpton, S. J.; Equilibration of long chain polymer melts in computer simulations. *J. Chem. Phys.* **2003**, *119*, 12718-12728.
- [53] Plimpton, S. Fast parallel algorithms for short-range molecular dynamics. J. Comp. Phys. 1995, 117, 1-19.
- [54] Casas, F; Alba-Simionesco, C; Montes. H; Lequeux, F; Length scale of glassy polymer plastic flow: a neutron scattering study. *Macromolecules* **2008**, *41*, 860.
- [55] Moghadam, S.; Dalal, I. S.; Larson, R. G. Slip-link and kink dynamics models for fast extensional flow of entangled polymeric liquids, *Polymer*, **2019**, *11*, 465.
- [56] Moghadam, S.; Dalal, I. S.; Larson, R. G. Unraveling dynamics of entangled polymers in strong extensional flows. *Macromolecules* **2019**, *52*, 1296-1307.

- [57] Govaert, L. E.; Tervoort, T. A.; Strain hardening of polycarbonate in the glassy state: Influence of temperature and molecular weight. *J. Polym. Sci Part B Polym. Phys. J. Polym. Sci Part B Polym. Phys.* **2004**, 42, 2041-49.
- [58] Riggleman, R. A.; Lee, H.-N.; Ediger, M. D. and de Pablo, J. J. Heterogeneous dynamics during deformation of a polymer glass. *Soft Matt.* **2010**, *6*, 287-291.
- [59] Lee, H.-N.; Paeng, K.; Swallen, S. F.; *et al.* Molecular mobility of poly(methyl methacrylate) glass during uniaxial tensile creep deformation. *J. Polym. Sci. B* **2009**, *47*, 1713-1727.
- [60] Lee, H.-N.; Paeng, K.; Swallen, S. F.; and Ediger, M. D. Direct measurement of molecular mobility in actively deformed polymer glasses. *Science* **2009**, *323*, 231-234.
- [61] Bending, B.; and Ediger, M. D. Comparison of mechanical and molecular measures of mobility during constant strain rate deformation of a PMMA glass. *J. Polym. Sci. B* **2016**, *54*, 1957-1967.
- [62] Lee, H.-N.; Riggleman, R. A.; de Pablo, J. J.; and Ediger, M. D. Deformation-induced mobility in polymeric glasses during multistep creep experiments and simulations. *Macromolecules* **2009**, *42*, 4328-4336.
- [63] Schweizer, K. S.; and Saltzmann, E. J. Theory of dynamic barriers, activated hopping and the glass transition in polymer melts. *J. Chem. Phys.* **2004**, *121*, 1984–2000.
- [64] Chen, K.; Saltzman, E. J.; and Schweizer, K. S. Segmental dynamics in polymers: from cold melts to ageing and stressed glasses. *J. Phys.: Condens. Matter* **2009**, *21*, 503101.
- [65] Thurau, C. T.; and Ediger, M. D. Influence of spatially heterogeneous dynamics on physical aging of polystyrene. *J. Chem. Phys.* **2002**, *116*, 9089–9099.
- [66] Caruthers, J. M.; Adolf, D. B.; Chambers, R. S.; Shrikhande, P. A thermodynamically consistent, nonlinear viscoelastic approach for modeling glassy polymers. *Polymer* **2004**, *45*, 4577-4597.
- [67] Cavaille, J. Y.; and Perez, J.; Johari, G. P. Molecular theory for the rheology of glasses and polymers. *Phys. Rev. B* **1989**, *39*, 2411-2422.
- [68] Pérez-Aparicio, R.; Cottinet, D.; Crauste-Thibierge, C.; *et al.* Dielectric spectroscopy of a stretched polymer glass: Heterogeneous dynamics and plasticity. *Macromolecules* **2016**, *49*, 3889-3898.
- [69] Dudowicz, J.; Douglas, J. F.; Freed, K. F. Advances in the generalized entropy theory of glass-formation in polymer melts. *J. Chem. Phys.* **2014**, *141*, 234903.